Journal of Computational and Applied Research in Mechanical Engineering
jcarme.sru.ac.ir
SRTTU
JCARME
ISSN: 2228-7922

Research paper

Modeling of dynamic cutting forces and cutting characteristics based on the analyzed results of average force-feed rate relationship in milling process

Nhu-Tung Nguyen[a,*], Pham Van Dong[b], Pham Duc Cuong[a] and Dung Hoang Tien[c]

[a]*HaUI Institute of Technology – HIT, Hanoi University of Industry, Hanoi city, 100000, Vietnam*
[b]*Science and Technology Department, Hanoi University of Industry, Hanoi city, 100000, Vietnam*
[c]*Mechanical Engineering Faculty, Hanoi University of Industry, Hanoi city, 100000, Vietnam*

Article info:

Article history:

Received: 20/04/2021
Revised: 27/10/2021
Accepted: 30/10/2021
Online: 03/11/2021

Keywords:

Dynamic cutting force,
Average cutting force,
Cutting characteristics,
Flat-milling process.

[*]Corresponding author:
tungnn@haui.edu.vn

Abstract

Cutting force coefficients (CFCs) are the most important factors in the prediction of CFs (CFs) and other machining characteristics (MCs). This study was conducted to model the CFs and MCs in the milling process based on the calculated values of CFCs. From the relationship of average values of CFs and feed rate, CFCs were determined and used to predict dynamic CFs (DCFs) in the flat milling process. In static models, the average values of CFs were presented as a linear regression of feed rate. The DCFs and other MCs were modeled depending on the cutting parameters, cutter geometry, CFCs, and structure parameters of the machine-tool system. By performing the flat-milling process of gray cast iron GG25 using HSS-Co solid tool, the average CFs were modeled as the linear regression of feed rate with large determination coefficients (R^2 > 93%). Besides, all CFCs of a pairs of tool and workpiece for each cutting type were successfully determined based on the measured data of CFs from the experimental process. Moreover, the proposed models of DCFs were successfully verified based on the compared results between the predicted CFs and measured CFs in several cutting tests with different cutting parameters. The proposed models of cutting force in this study were successfully used to predict the DCFs and several MCs in milling processes using a flat milling tool. And can be used to design and develop tools and machine in industrial manufacturing.

1. Introduction

In milling processes, the CFs are the most important components to predict the machining characteristics and improvement of quality and effective of the machining processes. The CFs can be predicted by two methods including, theoretical and experimental methods. In the experimental method, the cutting force models are modeled from experimental data with several controllable input parameters such as depth of cut, feed rate, and cutting velocity [1, 2]. It is

quite easy to perform this method; however, the CF models in these are often only used for specific cases of the machine, tool, workpiece, and even machining conditions. In theoretical methods of cutting force, the CFs are modeled based on the mechanical, geometrical, and tool-workpiece physical interactions in cutting processes. The orthogonal and oblique models were applied to analyze the cutting mechanics [3, 4]. In these cases, the relationship of chip thickness and cutting force based on the CFCs was applied to build the CF models. So, the effective method of CFCs is one of the most important keys to model the CFs in machining processes. The traditional approach in the determination of CFCs is that from the cutting test of each pair of tools and workpiece, the edge force coefficients and shear force coefficients are determined and evaluated. This approach has been applied conveniently in milling [4], turning [5], drilling [6], and grooving [7]. The transformation method and direct method are two methods that are often applied to determine CFCs. In the first one, CFCs were determined based on data that were obtained by orthogonal experimental processes [4, 8]. Based on the cutting force models for the oblique cutting process when considering the effect of the end of the cutting edge, the CFCs were also estimated [9]. In the second one, from cutting test data, CFCs were determined directly from several measured parameters such as the cutting edge length, the spindle speed, and the instantaneous values of the uncut chip thickness [10], from measured cutter deflection [11] and the instantaneous cutting force [12]. Besides, the measured average CFs were also used to calculate the CFCs [13].

In the direct calibration of CFCs, the CFCs were often determined using two models. The exponential force coefficients model is the first model that has been applied to determine CFCs. Using this model, CFCs were determined based on the measured values of the average chip thickness [14-18]. The second model is called the linear-force model that the CFCs were determined based on the values of the average cutting force. Using this model, the CFs were successfully modeled and verified in several milling processes such as in the milling using flat mill tool [2, 13], the milling process using ball mill tool [19], and the milling process using face mill tool [20].

The linear relationship of average CFs and feed rate was applied to determine CFCs in the flat milling process with the influence of the cutter's helix angle [21]. The stable cutting conditions were evaluated by the experimental method. Then, these stable cutting conditions were applied to determine the CFCs. However, only a half-down milling type was carried out to determine CFCs. Other cutting types as half-up milling and slotting have not been conducted to determine CFCs. Besides, the authors only investigated the static model forces, and the modeling process has not been mentioned for dynamic CFs in the milling process.

To evaluate the CFCs in different milling types, in this study, CFCs were estimated based on the regression model of average CFs in the flat milling process. Six components of CFCs were determined from the experimental data of CFs. The main contributions of this study are (1) successfully verifying the average CF models in all three cutting types (down milling, up milling, and slotting), (2) successfully determining the CFCs in these three cutting types, (3) successfully determining the parameters of the machine-tool dynamic structure system, and (4) successfully modeling and verifying the DCFs and predicting several MCs in flat milling processes.

2. Modeling of DCFs and MCs in flat milling process

2.1. DCF modeling

The cutter rotation angle and the CFs in the flat-milling process are ϕ_j, as presented in Fig. 1. The cutter rotation angle (degree) of flute number j (ϕ_j) was calculated by Eq. (1).

$$\phi_j = \phi_1 - (j-1)\phi_P,\ j = 1 \sim N_f \quad (1)$$

where ϕ_P is the distance angle of cutter number i and cutter number i-1 (degree). This angle depends on the cutter geometry, and it can be calculated by Eq. (2).

$$\phi_P = \frac{2\pi}{N_f} \quad (2)$$

At an axial depth of cut (z), the lag angle $\Psi_j(z)$ is expressed by Eq. (3), based on the effect of the cutter helix angle (β) [4, 21].

$$\Psi_j(z) = \frac{2\tan\beta}{D} z \tag{3}$$

where D is the diameter of cutting tool (mm).
The cutter rotation angle ($\phi_j(z)$) of the flute number j, at an axial depth of cut z was calculted by Eq. (4), as described in Fig. 1.

$$\phi_j(z) = \phi_j - \Psi_j(z) = \phi_1 - (j-1)\phi_P - \frac{2\tan\beta}{D} z \tag{4}$$

Assuming that with the new cutter, the cutter nose radius is equal to zero, the differential tangential CF (N), differential radial CF (N), and differential axial CF (N) were modeled in Eq. (5) [2, 21].

$$\begin{cases} dF_{t,j}(\phi_j, z) = K_{te} * dz + K_{tc} * h_j(\phi_j(z)) * dz \\ dF_{r,j}(\phi_j, z) = K_{re} * dz + K_{rc} * h_j(\phi_j(z)) * dz \\ dF_{a,j}(\phi_j, z) = K_{ae} * dz + K_{ac} * h_j(\phi_j(z)) * dz \end{cases} \tag{5}$$

where $K_{i,j}$ is the CFCs, and the instantaneous chip thickness is $h_j(\phi_j(z))$.
The linear relationship of the average cutting force model and feed rate was applied to determine CFCs ($K_{i,j}$) in milling processes using a flat milling tool [21]. The milling experiments were performed with the constant depth of cut, constant spindle speed, and with the change of feed rate in the determination of the CFCs, as described clearly by Kao et al [21]. By this way, the CFCs were estimated by Eq. (6).

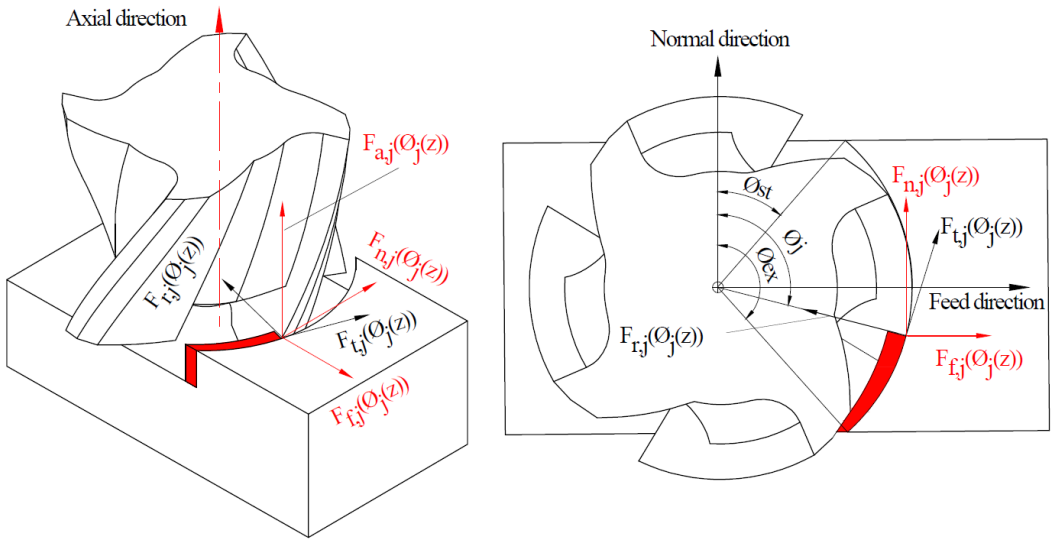

Fig. 1. Rotation angle and CFs in flat-milling process.

$$\begin{cases} C_1 = \frac{N_f}{4\pi}\left(-\int_{\phi_{st}}^{\phi_{st}+\Psi_a}\left[\int_0^{\frac{D}{2\tan\beta}(\phi-\phi_{st})}(\sin 2\phi_j(z))dz\right]d\phi - \int_{\phi_{st}+\Psi_a}^{\phi_{ex}}\left[\int_0^{a}(\sin 2\phi_j(z))dz\right]d\phi - \int_{\phi_{ex}}^{\phi_{ex}+\Psi_a}\left[\int_{\frac{D}{2\tan\beta}(\phi-\phi_{ex})}^{a}(\sin 2\phi_j(z))dz\right]d\phi\right) \\ C_2 = \frac{N_f}{4\pi}\left(-\int_{\phi_{st}}^{\phi_{st}+\Psi_a}\left[\int_0^{\frac{D}{2\tan\beta}(\phi-\phi_{st})}(1-\cos 2\phi_j(z))dz\right]d\phi - \int_{\phi_{st}+\Psi_a}^{\phi_{ex}}\left[\int_0^{a}(1-\cos 2\phi_j(z))dz\right]d\phi - \int_{\phi_{ex}}^{\phi_{ex}+\Psi_a}\left[\int_{\frac{D}{2\tan\beta}(\phi-\phi_{ex})}^{a}(1-\cos 2\phi_j(z))dz\right]d\phi\right) \\ C_3 = \frac{N_f}{2\pi}\left(-\int_{\phi_{st}}^{\phi_{st}+\Psi_a}\left[\int_0^{\frac{D}{2\tan\beta}(\phi-\phi_{st})}(\cos\phi_j(z))dz\right]d\phi - \int_{\phi_{st}+\Psi_a}^{\phi_{ex}}\left[\int_0^{a}(\cos\phi_j(z))dz\right]d\phi - \int_{\phi_{ex}}^{\phi_{ex}+\Psi_a}\left[\int_{\frac{D}{2\tan\beta}(\phi-\phi_{ex})}^{a}(\cos\phi_j(z))dz\right]d\phi\right) \\ C_4 = \frac{N_f}{2\pi}\left(-\int_{\phi_{st}}^{\phi_{st}+\Psi_a}\left[\int_0^{\frac{D}{2\tan\beta}(\phi-\phi_{st})}(\sin\phi_j(z))dz\right]d\phi - \int_{\phi_{st}+\Psi_a}^{\phi_{ex}}\left[\int_0^{a}(\sin\phi_j(z))dz\right]d\phi - \int_{\phi_{ex}}^{\phi_{ex}+\Psi_a}\left[\int_{\frac{D}{2\tan\beta}(\phi-\phi_{ex})}^{a}(\sin\phi_j(z))dz\right]d\phi\right) \\ C_5 = \frac{N_f}{2\pi}\left(\int_{\phi_{st}}^{\phi_{st}+\Psi_a}\left[\int_0^{\frac{D}{2\tan\beta}(\phi-\phi_{st})}dz\right]d\phi + \int_{\phi_{st}+\Psi_a}^{\phi_{ex}}\left[\int_0^{a}dz\right]d\phi + \int_{\phi_{ex}}^{\phi_{ex}+\Psi_a}\left[\int_{\frac{D}{2\tan\beta}(\phi-\phi_{ex})}^{a}dz\right]d\phi\right) \end{cases} \tag{7}$$

$$\begin{cases} K_{tc} = \frac{C_1\bar{F}_{fc} - C_2\bar{F}_{nc}}{C_1^2 + C_2^2} & K_{te} = \frac{C_3\bar{F}_{fe} - C_4\bar{F}_{ne}}{C_3^2 + C_4^2} \\ K_{rc} = \frac{C_2\bar{F}_{fc} + C_1\bar{F}_{nc}}{C_1^2 + C_2^2} & K_{re} = \frac{C_4\bar{F}_{fe} + C_3\bar{F}_{ne}}{C_3^2 + C_4^2} \\ K_{ac} = -\frac{\bar{F}_{ac}}{C_4} & K_{ae} = \frac{\bar{F}_{ae}}{C_5} \end{cases} \quad (6)$$

where C1, C2, C3, C4, and C5 are constants that can be calculated by Eq. (7) [20].
Besides, the average CFs are the average feed CF, average normal CF, and average axial CF ($\bar{F}_f$, $\bar{F}_n$, and $\bar{F}_a$) that were calculated from measured CFs with the change of feed rate.
The coefficients of the linear functions ($\bar{F}_{fc}$, $\bar{F}_{fe}$, $\bar{F}_{nc}$, $\bar{F}_{ne}$, $\bar{F}_{ac}$, and $\bar{F}_{ae}$) were determined by regressing the average CFs as the linear function of feed rate as presented in Eq. (8).

$$\begin{cases} \bar{F}_f = \bar{F}_{fc} f_t + \bar{F}_{fe} \\ \bar{F}_n = \bar{F}_{nc} f_t + \bar{F}_{ne} \\ \bar{F}_a = \bar{F}_{ac} f_t + \bar{F}_{ae} \end{cases} \quad (8)$$

2.2. Modeling of dynamic chip thickness and machining characteristics

The instantaneous chip thickness ($h_j(\phi_j(z))$) consists of the static chip thickness, chip thickness from cutter run-out, and the dynamic chip thickness. So, Eq. (9) was applied to calculate the instantaneous chip thickness.

$$h_j\left(\phi_j(z)\right) = h_s\left(\phi_j(z)\right) + h_{run-out}\left(\phi_j(z)\right) + h_d\left(\phi_j(z)\right) \quad (9)$$

In static status (without vibration), the static chip thickness (Fig. 2) is a function of feed per flute and cutter rotation angle as presented by Eq. (10).

$$h_s\left(\phi_j(z)\right) = f_t \sin\left(\phi_j(z)\right) \quad (10)$$

Considering with a new tool, the run-out parameters of the tool are equal to zero. The chip thickness (mm) that is formed from run-out parameters is also equal to zero ($h_{run-out}\left(\phi_j(z)\right) = 0$).

Fig. 3 described the formation of dynamic chip thickness. This parameter can be calculated by Eq. (11).

$$h_d\left(\phi_j(z)\right) = w_t(\phi_j) - w_{(t-\tau)}(\phi_j) \quad (11)$$

where $w_t(\phi_j)$ and $w_{(t-\tau)}(\phi_j)$ are the displacement of flute number j and flute number i-1 at rotation angle $\phi_j(z)$ and can be calculated by Eq. (12).

$$\begin{cases} w_t(\phi_j(z)) = x_t \sin(\phi_j(z)) + y_t \cos(\phi_j(z)) \\ w_{(t-\tau)}(\phi_j(z)) = x_{(t-\tau)} \sin(\phi_j(z)) + y_{(t-\tau)} \cos(\phi_j(z)) \end{cases} \quad (12)$$

where x_t and $x_{(t-\tau)}$ are the vibrations of machine tool at time t and time $(t-\tau)$ in x directions, respectively, and y_t and $y_{(t-\tau)}$ are the vibrations of machine tool at time t and time $(t-\tau)$ in y directions, respectively.

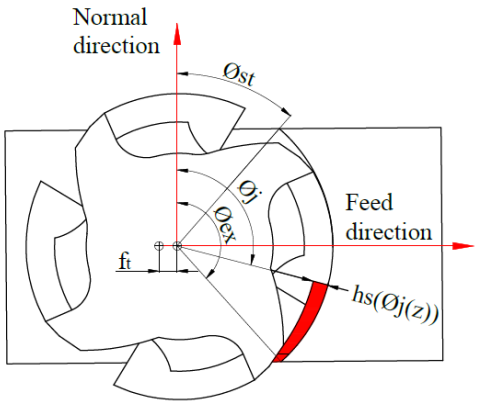

Fig. 2. The static chip thickness in flat-milling process.

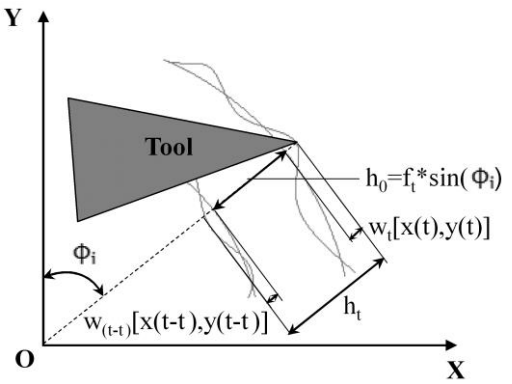

Fig. 3. The dynamic chip thickness in flat-milling process.

The vibration displacements of machine-tool in x and y directions were modeled by Eq. (13) [22-24].

$$\begin{cases} [m_x]\{\ddot{x}(t)\} + [c_x]\{\dot{x}(t)\} + [k_x]\{x\} = \{F_x(t)\} \\ [m_y]\{\ddot{y}(t)\} + [c_y]\{\dot{y}(t)\} + [k_y]\{y\} = \{F_y(t)\} \end{cases} \quad (13)$$

where $[m_j]$, $[c_j]$, and $[k_j]$ are the matrices of mass, damping coefficient, and system stiffness of machine tool system, respectively, in the j direction, as shown in Fig. 4. These matrices are often determined by analyzing the frequency response function that was obtained by the experimental method for each machine-tool system.

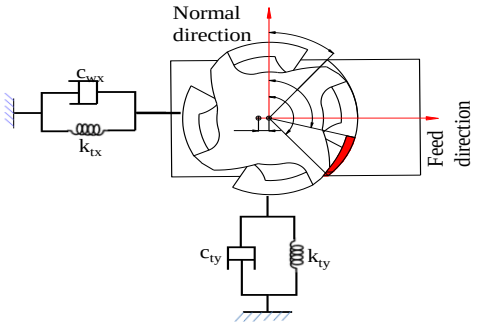

Fig. 4. Machine tool dynamic structure in flat-milling process.

The DCFs are modeled depending on the process, as shown in Fig. 5, and can be presented as follows:

Step 1: Calculate the chip thickness (first time, it is the initial value or the static chip thickness);
Step 2: Calculate the tangential, radial, and axial differential CFs;
Step 3: Calculate the feed, normal, and axial differential CFs;
Step 4: Calculate the total CFs in feed, normal, and axial directions;
Step 5: Calculate the x and y vibrations.

From step 5, the obtained vibrations will be one of the output parameters for the calculation of chip thickness. So, this process is a close loop. Other MCs such as cutting power, bending moment, torque moment, etc., were calculated depending on the values of calculated CFs.
The tangential, radial, and axial differential DCFs were calculated by Eq. (14).

$$\begin{cases} dF_{t,j}(\phi_j, z) = [K_{tc} h_j(\phi_j(z)) + K_{te}] * dz \\ dF_{r,j}(\phi_j, z) = [K_{rc} h_j(\phi_j(z)) + K_{re}] * dz \\ dF_{a,j}(\phi_j, z) = [K_{ac} h_j(\phi_j(z)) + K_{ae}] * dz \end{cases} \quad (14)$$

The feed, normal, and axial differential DCFs were calculated using the transformation as in Eq. (15).

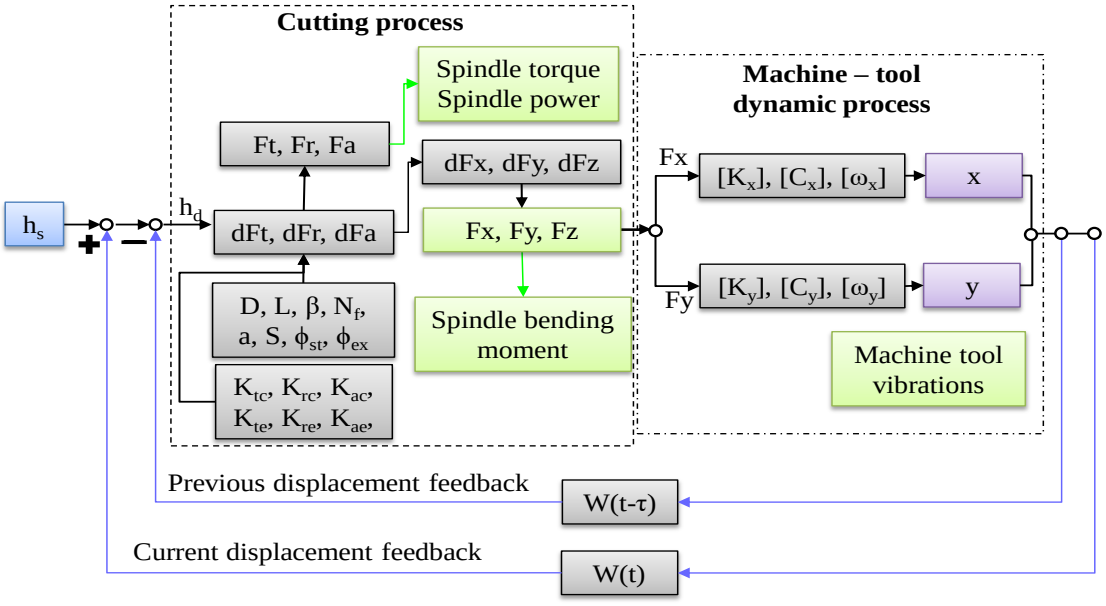

Fig. 5. The block diagram of dynamic milling process.

$$\begin{Bmatrix} dF_{f,j}(\phi_j,z) \\ dF_{n,j}(\phi_j,z) \\ dF_{a,j}(\phi_j,z) \end{Bmatrix} = \begin{bmatrix} -\cos(\phi_j(z)) & -\sin(\phi_j(z)) & 0 \\ \sin(\phi_j(z)) & -\cos(\phi_j(z)) & 0 \\ 0 & 0 & 1 \end{bmatrix} \begin{Bmatrix} dF_{t,j}(\phi_j,z) \\ dF_{r,j}(\phi_j,z) \\ dF_{a,j}(\phi_j,z) \end{Bmatrix} \quad (15)$$

The differential DCFs of each cutting edge on the cutter flute were calculated by Eq. (16).

$$F_{q,j}(\phi_j) = \int_{z_1(\phi_j)}^{z_2(\phi_j)} dF_{q,j}(\phi_j,z), \quad q = f,n,a \quad (16)$$

where $z_1(\phi_j)$ and $z_2(\phi_j)$ are the minimum and maximum depth of cut of each cutting edge, respectively.
The boundary conditions in the calculation of CFs were determined as the beginning and ending cutter rotation angles of each cutting edge, as presented in Eq. (17).

$$\phi_{st} \le \phi_j \le \phi_{ex} + \Psi_a \quad (17)$$

where ϕ_{st} and ϕ_{ex} are the entry and exit angles of each cutting edge, respectively. Ψ_a is the lag angle at a maximum depth of cut as calculated by Eq. (18).

$$\Psi_a = \frac{2\tan\beta}{D}a \quad (18)$$

where a is the maximum depth of cut.
The total feed, normal, and axial DCFs were calculated by Eq. (19).

$$\begin{cases} F_f(\phi_j) = \sum_{j=1}^{N_f} F_{f,j}(\phi_j) \\ F_n(\phi_j) = \sum_{j=1}^{N_f} F_{n,j}(\phi_j) \\ F_a(\phi_j) = \sum_{j=1}^{N_f} F_{a,j}(\phi_j) \end{cases} \quad (19)$$

In this study, the feed, normal, axial directions coincide with x, y, and z directions, so the CFs in x, y, z, and the resultant cutting force in xy plane $F_{xy}(\phi_j)$ can be calculated by Eq. (20).

$$\begin{cases} F_x(\phi_j) = F_f(\phi_j) \\ F_y(\phi_j) = F_n(\phi_j) \\ F_z(\phi_j) = F_a(\phi_j) \\ F_{xy}(\phi_j) = \sqrt{F_x^2(\phi_j) + F_y^2(\phi_j)} \end{cases} \quad (20)$$

From the calculation results of dynamic CFs, other machining characteristics such as the spindle power, spindle torque, and spindle bending moment can also be modeled.
The spindle power $P(\phi_j)$ can be calculated by Eq. (21).

$$P(\phi_j) = 10^{-6} V_c \sum_{j=1}^{N_f} F_{t,j}(\phi_j) \quad (21)$$

where V_c is the cutting velocity that can be calculated by Eq. (22).

$$V_c = \frac{\pi DS}{1000} \quad (22)$$

where S is the spindle speed.
The spindle torque $T(\phi)$ can be calculated by Eq. (23).

$$T(\phi_j) = 10^{-3} \frac{D}{2} \sum_{j=1}^{N_f} F_{t,j}(\phi_j) \quad (23)$$

The spindle bending moment $M(\phi_j)$ can be calculated by Eq. (24).

$$M(\phi_j) = 10^{-3} L F_{xy}(\phi_j) \quad (24)$$

where L is the tool length.

3. Material and experimental method

3.1. Material

To verify the average CF models as presented by Eq. (8) and verify the DCF models, the experiments were performed in flat milling processes of gray cast iron GG25 using a solid flat mill tool.
The gray cast iron GG25 is known as one of the least expensive metals of all cast metals. This metal is often considered first when a cast metal is selected because of the low cost of its metal. The machinability of the gray cast iron GG25 is superior to that of virtually all steels because of the graphite present. The workpiece dimensions were the length of 80 mm, the width of 30 mm, and the height of 40 mm, as shown in Fig. 6.
The flat solid milling tool was chosen with main properties as follows: flute number (N_f) of 2 flutes, helix angle (β) of 30^0, rake angle (α_r) of 5^0, and cutter diameter (D) of 10 mm. A high-speed steel tool that was coated by Co (HSS-Co) was used in cutting tests, as described in Fig. 7.

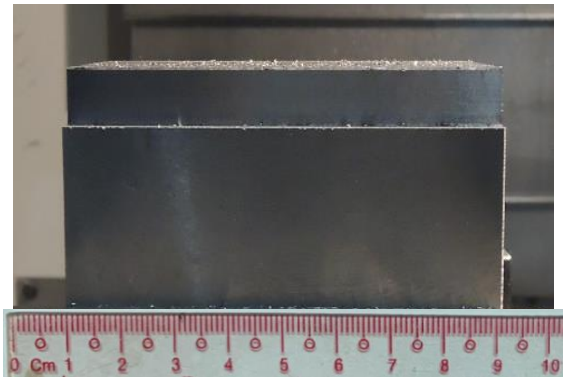

Fig. 6. Experimental workpiece.

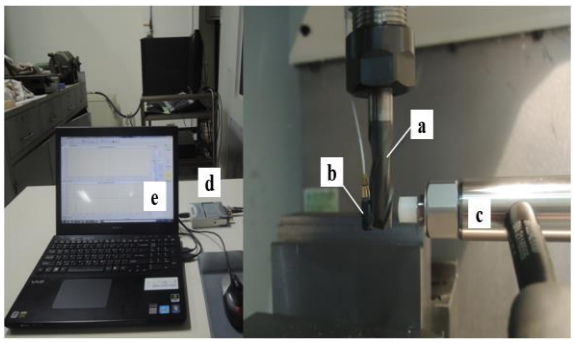

Fig. 7. Setting of machine tool dynamic structure measurement; (a) tool, (b) acceleration sensor, (c) force sensor, (d) signal processing box, and (e) Cutpro™ software.

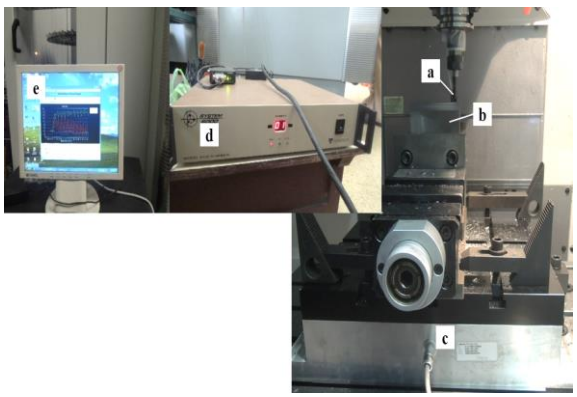

Fig. 8. CF measurement; (a) tool, (b) workpiece, (c) dynamometer, (d) processing system, and (e) software.

3.2. Machine and determination method of machine-tool structure parameters

TWV-720A CNC milling machine was used to conduct the cutting tests as described in Fig. 8. The machine-tool dynamic structure parameters were determined by a measurement system including the Endevco-25B-10668 acceleration sensor, Kistler-9722A2000 force sensor, Ni-9234 signal processor, and Cutpro™ software, as described in Fig. 7.

3.3. DCF measurement system

The DCFs were measured in feed (x), normal (y), and axial (z) directions using a measurement system including a 624-120-5KN CF sensor (XYZ directions), a processing system, and an application software. Fig. 8 presented the detail of CFs measurement system.

3.4. Experimental plan

The cutting tests include two sets. Set 1 was performed to determine the CFCs. In this set, half-up milling tests, half-down milling tests, and slotting tests were conducted with constant cutting depth, constant spindle speed, and variations of feed rate. The cutting tests were conducted with small values of cutting depth and spindle speed to ensure stable conditions [22, 25]. Set 2 was conducted at the normal cutting conditions with different cutting types and different cutting conditions to measure DCFs and evaluate the DCF models. The experimental parameters of all cutting tests were presented in Table 1.

Table 1. Cutting test parameters.

Test No	Cutting type	a (mm)	S (rpm)	ft (mm/flute)
Set 1: Verification of average force model and determination of cutting force coefficients				
1	Half-down	0.5	1000	0.050
2	Half-down	0.5	1000	0.075
3	Half-down	0.5	1000	0.100
4	Half-down	0.5	1000	0.150
5	Half-down	0.5	1000	0.200
6	Half-up	0.5	1000	0.050
7	Half-up	0.5	1000	0.075
8	Half-up	0.5	1000	0.100
9	Half-up	0.5	1000	0.150
10	Half-up	0.5	1000	0.200
11	Slotting	0.5	1000	0.050
12	Slotting	0.5	1000	0.075
13	Slotting	0.5	1000	0.100
14	Slotting	0.5	1000	0.150
15	Slotting	0.5	1000	0.200
Set 2: Verification of dynamic cutting force model				
16	Half-down	1.5	2000	0.100
17	Half-up	1.5	2000	0.100
18	Slotting	1.0	3000	0.100

4. Experimental results and discussions

4.1. Analysis of machine-tool structure parameters

Using the dynamic structure measurement system, the force and response vibration in the tapper test was stored for each direction of the machine tool system. By using the measured results, the relationship of force and response vibration was analyzed in the frequency domain as the frequency response function (FRF). Then, based on obtained FRF, Cutpro^{TM} software was applied to de structure parameters of a machine-tool system.

The analyzed FRF results of the dynamic structure of the machine-tool system is described in Fig. 9. Table 2 presents the obtained results of the dynamic structure parameters of this machine-tool system.

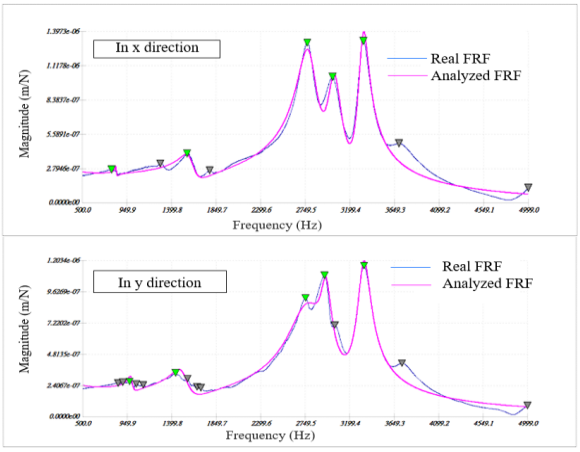

Fig. 9. Analysis of machine-tool dynamic structural.

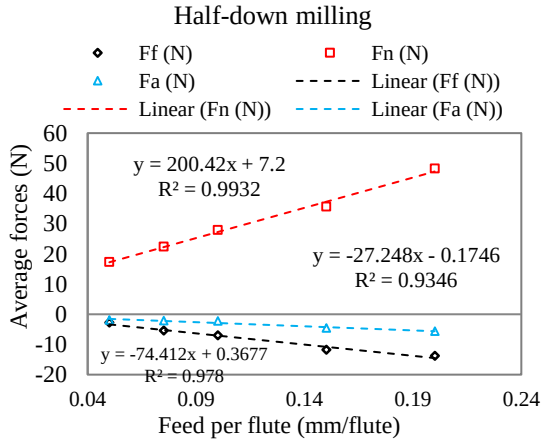

Fig. 10. Regression models of average CFs in half-down.

The obtained results showed that the dynamic structures of the different directions are different. It means that the effects of the dynamic process on the cutting process in different directions are different.

Besides, in the same dynamic structure mode of the machine tool system, the structure natural frequencies in different directions are quite close to each other but not the same. This difference is 15.01 % in this machine tool system. It means that in one machine tool system, the effect of the natural frequency of the machine tool system on the cutting process is different in different directions, but this difference is not so much. The experimental method by using Cutpro^{TM} software is a convenient method to determine the structure parameters of a machine-tool system.

4.2. Average CFs and CFCs

The average CFs were calculated from measured data of CFs set 1 as listed in Table 3. The results from this figure show very clearly that the average CFs changed with the change of feed per flute in all cutting types and all directions. The results in Table 3 also show that the average CFs in different directions can be negative or positive values. This issue can be explained as follows:

In this study, the CFs that were modeled are the instantaneous CFs, the instantaneous CFs are built as a mathematical and trigonometric (sine, cosine) function of many parameters whose one of these parameters is the rotational position of the cutting tool in the milling process.

The rotating position of the cutting tool changes cyclically from 0 degrees to 360 degrees in milling processes; therefore, the instantaneous cutting force values can be also the negative or positive values in different directions. This leads to the average cutting force values can also be negative or positive values in different directions.

The regression models of average CFs were investigated and described from Figs. 10 to 12. The obtained results from these figures show that for all milling types in this study (half-down, half-up, and slotting), the average cutting force is a linear regression of the feed rate with large determination coefficients (more than 93.46%). So, in flat milling processes, the average CFs can be modeled as the linear regression of the feed rate not only for one milling type [2, 20, 24] but also for different cutting types.

Table 2. Structure parameters of machine-tool dynamic system.

Direction	Mode No.	Natural frequency (Hz)	Damping ratio (%)	Modal stiffness (N/m)	Mass (kg)
X	1	842.975	0.898	7.8919E+08	28.132
	2	1591.739	5.067	4.8211E+07	0.482
	3	2790.641	3.940	1.2730E+07	0.041
	4	3040.326	2.447	2.7212E+07	0.075
	5	3331.161	1.683	2.5056E+07	0.057
Y	1	991.800	2.641	1.8614E+08	4.793
	2	1514.482	6.180	4.0318E+07	0.445
	3	2785.8612	6.635	1.3818E+07	0.0451
	4	2960.7592	1.996	4.4508E+07	0.1286
	5	3342.8788	2.054	2.2508E+07	0.0569

Table 3. The average CFs.

ft (mm/flutes)	Half-down			Half-up			Slotting		
	Ff (N)	Fn (N)	Fa (N)	Ff (N)	Fn (N)	Fa (N)	Ff (N)	Fn (N)	Fa (N)
0.050	-2.820	17.301	-1.953	20.223	9.375	-3.941	-29.413	56.557	-11.479
0.075	-5.474	22.334	-2.131	25.958	11.916	-4.691	-32.663	78.774	-12.453
0.100	-7.054	27.832	-2.219	29.295	13.087	-5.067	-48.526	91.653	-18.320
0.150	-11.779	35.584	-4.592	41.762	18.315	-8.845	-55.955	119.771	-27.604
0.200	-13.821	48.188	-5.645	49.632	22.065	-10.322	-68.840	159.541	-29.259

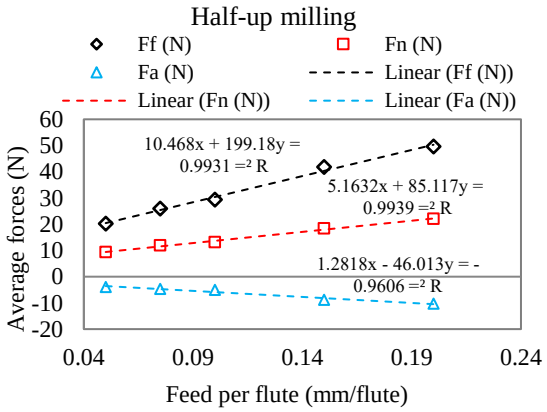

Fig. 11. Regression models of average CFs in half-up.

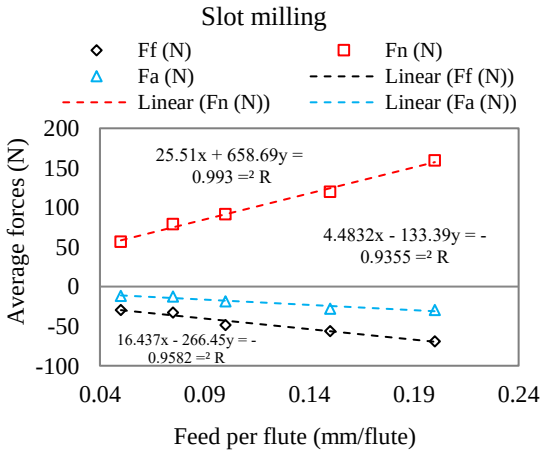

Fig. 12. Regression models of average CFs in slotting.

The analyzed results show that the measured results of average CFs have a good agreement with the analyzed results from theoretical models of average CFs. So, in the flat milling process, the average CFs can be presented as the linear regression of the feed rate.

Using average cutting force data, all six CFCs were determined by applying Eq. (6) and listed in Table 4. The obtained results in this figure show that the CFCs are different when determined in different cutting types. The absolute values of edge force coefficients (K_{te}, Kr_e, and K_{ae}) are much smaller than those of shear force coefficients (K_{tc}, K_{rc}, and K_{ac}).

Besides, in each cutting type, the absolute value of K_{tc} is the largest in all CFCs. Moreover, K_{ac} is often the smallest value in all CFCs.

Table 4. Obtained CFCs

Cutting types	Shearing force coefficient (N/mm²)		
	K_{tc}	K_{rc}	K_{ac}
Half-down	1320.631	223.272	-134.378
Half-up	1224.800	863.381	-283.039
Slotting	1316.300	532.900	-206.167
Cutting types	Edge force coefficient (N/mm)		
	K_{te}	K_{re}	K_{ae}
Half-down	24.218	30.816	-3.488
Half-up	46.322	14.144	-5.252
Slotting	37.877	26.320	-5.010

4.3. Predicted results of DCFs

The DCFs were predicted using the obtained CFCs in Table 4 and cutting parameters in Table 1 to compare to the experimental DCFs. The compared results are described from Figs. 13 to 15 for different cutting types and different cutting parameters of Set 2. With different cutting types and different cutting parameters, the DCFs predicted were quite close to the one from the experimental process. There are some different points between predicted and measured DCFs. These differences were quite small, as highlighted by circles from Figs. 13 to 15.

The predicted DCFs were the solid lines that were not the same as the dotted lines (measured dynamic CFs) in every revolution. The amplitude of predicted dynamic CFs is sometimes larger and sometimes smaller than the amplitude of measured DCFs. Besides, the shapes of DCFs are often different in different revolutions. In this study, there are some different points between predicted DCFs and measured DCFs. But the differences are quite small. Besides, the shape of the predicted DCFs is close to the measured ones and the amplitude of predicted DCFs has a little difference to that one of the measured DCFs.

The cutter run-out, noise, temperature, friction, deflection, etc., can be the reasons for the above differences.

From the above-analyzed results, it can be concluded that the predicted results of DCFs are quite close to the measured DCF results. So, the proposed DCF models in this study can be applied to predict DCFs and other MCs such as vibrations, cutting power, bending moment, etc., in milling processes using the flat milling tool.

4.4. Predicted results of MCs

DCFs and other MCs such as chip thickness, machine tool vibrations, spindle power, spindle torque, etc., were predicted based on the obtained results of CFCs, the structure parameters of the machine-tool system, and the proposed DCF models. Fig. 16 presents the predicting process of machining characteristics in the flat milling process.

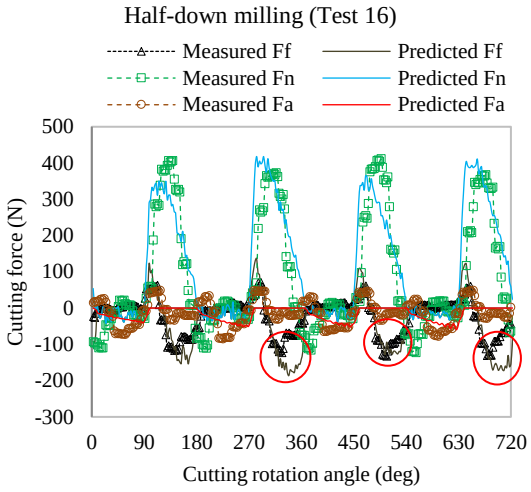

Fig. 13. Evaluation of DCFs in half-down milling.

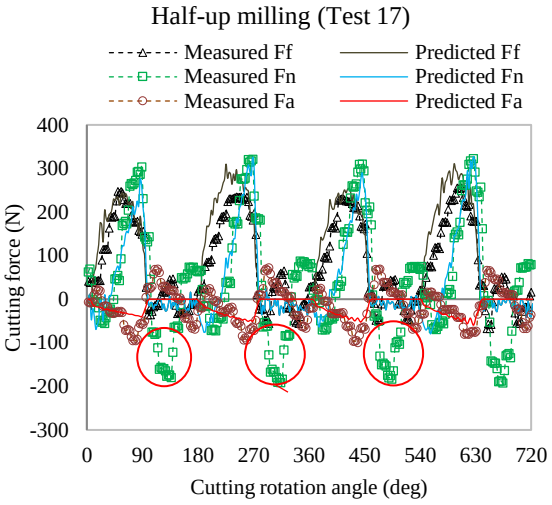

Fig. 14. Evaluation of DCFs half-up milling.

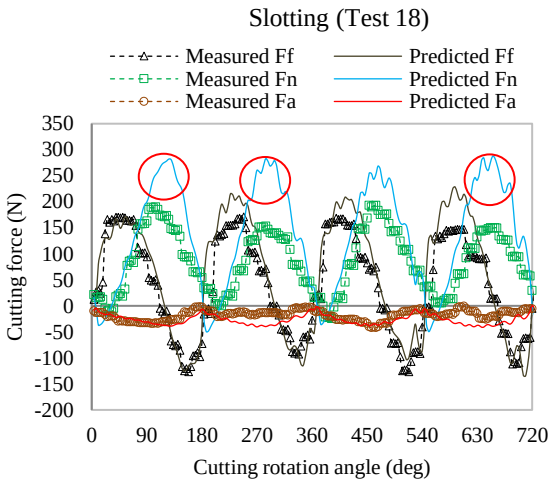

Fig. 15. Evaluation of DCFs in slotting.

The input parameters of the prediction system consist of tool properties such as tool diameter, tool length, number of flutes, helix angle, tool material, properties of the workpiece, cutting parameters, the system natural frequency, system stiffness, coefficient of damping, and so on.

The output parameters are the machining characteristics of dynamic chip thickness, DCFs, vibrations, spindle power, etc., which were predicted and illustrated in Fig. 17. These parameters are expected to apply in the designing and development of tools and machines in industrial manufacturing.

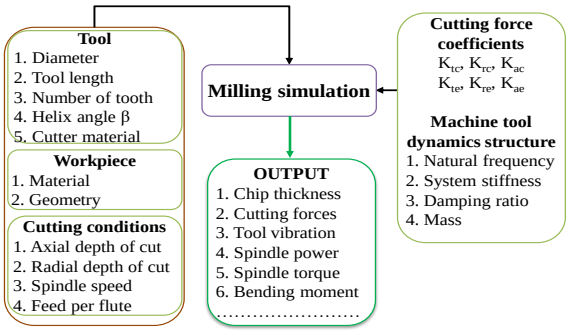

Fig. 16. Approach to prediction of machining characteristics.

6. Conclusions

From the analyzed results in the flat milling process of gray cast iron GG25 using a solid HSS-Co tool, the conclusions were drawn as follows:

- The dynamic structures of the different directions are different. It means that the effects of the dynamic process on the cutting process in different directions are different.
- In stable milling conditions with different types, the average CFs can be presented as the linear regression of the feed rate with the determination coefficient $R^2 > 93\%$.
- All six CFCs were determined based on the regression of average CFs. CFCs were different when determined in different cutting types.
- The shape of the predicted DCFs is close to the measured one and the amplitude of predicted DCFs has a little difference to that one of the measured CFs.
- The proposed models of DCFs were successfully applied to predict the DCFs, vibrations, cutting power, bending moment, spindle torque, etc., in milling processes using a flat milling tool. These models can be used to design and develop tools and machines in industrial manufacturing. Development, verification, and application of cutting force models for other machining processes will be the further works of this study.

Acknowledgment

This study was supported by the research project grant number 02-2020-RD/HĐ-ĐHCN of Hanoi University of Industry, Vietnam.

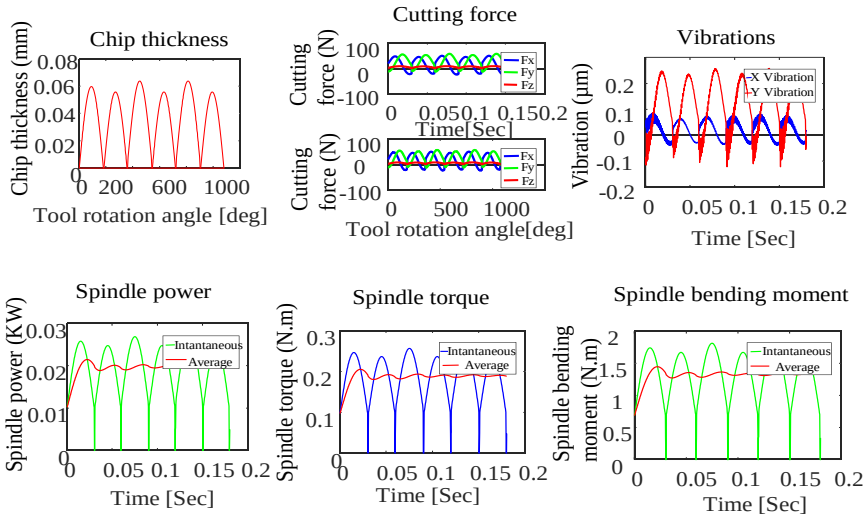

Fig. 17. The prediction of cutting characteristics.

References

[1] T. D. Hoang, N. T. Nguyen, D. Q. Tran and V. T. Nguyen, "CFs and Surface Roughness in Face-Milling of SKD61 Hard Steel", *Strojniski Vestnik/J. Mech. Eng.*, Vol. 65, No. 6, pp. 375-385, (2019).

[2] L. Imani, A. R. Henzaki, R. Hamzeloo and B. Davoodi, "Modeling and optimizing of cutting force and surface roughness in milling process of Inconel 738 using hybrid ANN and GA", *Proc. Inst. Mech. Eng., Part B: J. Eng. Manuf.*, Vol. 234, No. 5, pp. 920-932, (2020).

[3] M. E. Merchant, "Mechanics of the Metal Cutting Process. I. Orthogonal Cutting and a Type 2 Chip", *J. Appl. Phys.*, Vol. 16, No. 5, pp. 267-275, (1945).

[4] Y. Altintas, *Manufacturing Automation: Metal cutting mechanics, machine tool vibrations, and CNC design*. Cambridge University Press, 2nd ed, ISBN 978-1-00148-0, (2012).

[5] A. I. Fernández-Abia, J. Barreiro, L. N. L. de Lacalle and S. Martínez-Pellitero, "Behavior of austenitic stainless steels at high-speed turning using specific force coefficients", *Int. J. Adv. Manuf. Technol.*, Vol. 62, No. 5-8, pp. 505–515, (2012).

[6] N. Guibert, H. Paris and J. Rech, "A numerical simulator to predict the dynamical behavior of the self-vibratory drilling head", *Int. J. Mach. Tools Manuf.*, Vol. 48, No. 6, pp. 644–655, (2008).

[7] J. M. Lee, T. J. Je, D. S. Choi, S. W. Lee, D. Le and S. J. Kim, "Micro grooving simulation and optimization in the roughing stage", *Int. J. Precis. Eng. Manuf.*, Vol. 11, No. 3, pp. 361-368, (2010).

[8] E. Budak, Y. Altintas and E. J. A. Armarego, "Prediction of milling force coefficients from orthogonal cutting data", *J. Manuf. Sci. Eng.*, Vol. 118, No. 2, pp. 216-224, (1996).

[9] X. P. Li and H. Z. Li, "Theoretical modelling of CFs in helical end milling with cutter run-out", *Int. J. Mech. Sci.*, Vol. 46, No. 9, pp.1399-1414, (2004).

[10] P. J. Cheng, J. T. Tsay and S. C. Lin, "A study on instantaneous cutting force coefficients in face milling", *Int. J. Mach. Tools Manuf.*, Vol. 37, No. 10, pp.1393-1408, (1997).

[11] A. Larue and B. Anselmetti, "Deviation of a machined surface in flank milling", *Int. J. Mach. Tools Manuf.*, Vol. 43, No. 2, pp. 129-138, (2003).

[12] A. Azeem, H. Y. Feng and L. Wang, "Simplified and efficient calibration of a mechanistic cutting force model for ball-end milling", *Int. J. Mach. Tools Manuf.*, Vol. 44, No. 2, pp. 291-298, (2004),

[13] M. Wang, L. Gao and Y. Zheng, "An examination of the fundamental mechanics of cutting force coefficients", *Int. J. Mach. Tools Manuf.*, Vol. 78, pp. 1-7, (2014).

[14] M. Wan, M. S. Lu, W. H. Zhang and Y. Yang, "A new ternary-mechanism model for the prediction of CFs in flat end milling", *Int. J. Mach. Tools Manuf.*, Vol. 57, pp. 34 – 45, (2012).

[15] J. W. Dang, W. H. Zhang, Y. Yang and M. Wan, "Cutting force modeling for flat end milling including bottom edge cutting effect", *Int. J. Mach. Tools Manuf.*, Vol. 50, No. 11, pp. 986-997, (2010).

[16] M. Wan, W. H. Zhang, J. W. Dang and Y. Yang, "A novel cutting force modeling method for cylindrical end mill", *Appl. Math. Modell.*, Vol. 34, No. 3, pp. 823-836, (2010).

[17] A. Bhattacharyya, J. K. Schueller, B. P. Mann, J. C. Ziegert, T. L. Schmitz, F. J. Taylor and N. G. Fitz-Coy, "A closed form mechanistic cutting force model for helical peripheral milling of ductile metallic alloys", *Int. J. Mach. Tools Manuf.*, Vol. 50, No. 6, pp. 538-551, (2010).

[18] Y. C. Kao, N. T. Nguyen, M. S. Chen and S. C. Huang, "A combination method of the theory and experiment in determination of cutting force coefficients in ball-end mill processes", *J. Comput. Des. Eng.*, Vol. 2, No. 4, pp. 233-247, (2015).

[19] J. Gradišek, M. Kalveram and K. Weinert, "Mechanistic identification of specific force coefficients for a general end mill", *Int. J. Mach. Tools Manuf.*, Vol. 44, No. 4, pp. 401-414, (2004).

[20] I. G. Euan, E, Ozturk and N. D. Sims. (2013). Modeling Static and Dynamic CFs and Vibrations for Inserted Ceramic

Milling Tools. Procedia CIRP, 8, pp. 564-569, (2013).
[21] Y. C. Kao, N. T. Nguyen, M. S. Chen and S. T. Su, "A prediction method of cutting force coefficients with helix angle of flat-end cutter and its application in a virtual three-axis milling simulation system", *Int. J. Adv. Manuf. Technol.*, Vol. 77, No. 9-12, pp. 1793-1809, (2015).
[22] Q. Cao, J. Zhao, Y. Li and L. Zhu, "The effects of cutter eccentricity on the cutting force in the ball-end finish milling", *Int. J. Adv. Manuf. Technol.*, Vol. 69, No. 9-12, pp. 2843-2849, (2013).
[23] C. H. Lee, M. Y. Yang, C. W. Oh, T. W. Gim and J. Y. Ha, "An integrated prediction model including the cutting process for virtual product development of machine tools", *Int. J. Mach. Tools Manuf.*, Vol. 90, pp. 29–43, (2014).
[24] A. Agarwal and K. A. Desai, "Importance of bottom and flank edges in force models for flat-end milling operation", *Int. J. Adv. Manuf. Technol.*, Vol. 107, No. 3, pp.1437-1449, (2020).
[25] N. T. Nguyen, *Modeling of Machining Dynamics: CFs and Machining Characteristics in Three-Axis Milling Processes*. Science and technics publishing House, Hanoi, Vietnam, (2020).

How to cite this paper:

Nhu-Tung Nguyen, Pham Van Dong, Pham Duc Cuong and Dung Hoang Tien, "Modeling of dynamic cutting forces and cutting characteristics based on the analyzed results of average force-feed rate relationship in milling processing,", *J. Comput. Appl. Res. Mech. Eng.*, Vol. 12, No. 1, pp. 63-75, (2022).

DOI: 10.22061/JCARME.2021.8011.2070

URL: https://jcarme.sru.ac.ir/?_action=showPDF&article=1620